COMMUNICATION

Flexible and Transparent Nanogenerators Based on a Composite of Lead-Free ZnSnO₃ Triangular-Belts

Jyh Ming Wu, Chen Xu, Yan Zhang, Ya Yang, Yusheng Zhou, and Zhong Lin Wang*

Technologies that harvest energy from the environment hold great promise for our daily lives. Recently, much attention to multiferroic materials has caused renewed interest in Pb-containing perovskites with transition metals[1,2] as they show excellent piezoelectric properties in ferroelectric, lead-oxide-based materials.[3] Despite some success in demonstrating an acceptable performance for diverse devices such as high frequency transducers,[4] energy harvesting nanogenerators,[5] and sensors,[6] all using $Pb(Zr,Ti)O_3$ (also called PZT), current technologies are still far from the ideal goal of having lead-free groups with varied applications. In order to apply biocompatible and environmentally friendly strategies to energy scavenging technologies, it is important to develop a lead-free piezoelectric material that can be used to build a self-powered nanodevice or -system.[3] A consistent effort has been made in developing the noncentrosymmetric (NCS) oxide group for the application of piezotronic devices.[7] One promising NCS oxide material called ZnO has received significant interest in the past decade because of its unique optoelectronic and piezoelectric properties.[8] The tuning effect of piezopotential can be used to control the charge transport properties across an interface of ZnO nano- or microwires. Our previous research relied on this tuning effect to discover a large variety of piezotronic devices.[9–13] Taking into consideration green energy and maintainance-free applications for healthcare, personal electronics, and environmental monitoring,[14] we have created a nanogenerator that is able to power a nanosystem or -devices by employing lead-free ZnO[15] and $NaNbO_3$[16] nano- or microwires. The advantage of using nano- or microwires for energy harvesting is that they can be fabricated into miniature devices with high mechanical robustness and responsiveness over a range of frequencies.

Recently, special attention has been paid to a high-performance, lead-free material called R3C $ZnSnO_3$[17,18] because its piezoelectric coefficient along its z-axis is ≈59 μCcm^{-2},[19] 12 times higher than that of ZnO ≈5 μCcm^{-2}.[20] In our previous work,[21] a single $ZnSnO_3$ microbelt nanogenerator achieved an output voltage and current of 100 mV and 30 nA, respectively. The excellent piezoelectric properties of $ZnSnO_3$ can be explained

by the fact that the displacement of the Zn atom in the ZnO_6 octahedral cell is almost two times that of the Sn atom in the SnO_6 octahedral cell, resulting in a large spontaneous polarization effect that naturally forms in the crystal structure along the z-axis.

This work describes a robust and cost-effective nanogenerator made from lead-free $ZnSnO_3$ triangular-belts with poly(dimethylsiloxane) (PDMS) film. A maximum output current and voltage reaches 0.13 μA and 5.3 V, respectively, corresponding to a output power of ≈11 μW·cm^{-3}. The process is very simple compared to other generally well-aligned nanowire technologies. The nanogenerator was fabricated by the integration of thousands of triangular-belt $ZnSnO_3$. Interestingly, one side of the triangular-belt naturally grew to be thicker than the other side during the crystal growth process. Due to the spontaneous polarization of $ZnSnO_3$ belts along the z-axis [001],[22] the unique geometric figure of highly dispersed triangular-belts caused their unipolar assembly to be located perpendicular to the surface of the substrate (e.g. P_{zy} direction). Therefore, the unipolar assembly of triangular-belts formed a substantial piezoelectric potential across the nanogenerator's thickness due to a compressive strain of ≈0.1%. This piezoelectric potential induced charges across the surfaces of the top and bottom electrodes. A theoretical estimate of piezopotential from the top electrode to the bottom electrode is 0.3–3 V. By increasing the intensity of triangular-belts in the nanogenerator, the output current and voltage increase accordingly. The experimental data exhibited consistency with our theory. The composite triangular-belt nanogenerator is highly transparent and flexible, demonstrating that $ZnSnO_3$ is a useful, lead-free material for piezoelectrical energy harvesting.

The details of the synthesis process for the triangular-belts are given in the Experimental Section. **Figure 1**a shows that the belt-like $ZnSnO_3$ were grown on Si substrates. The $ZnSnO_3$ triangular belt grew to up to 800 μm in length (with an average length of 200–300 μm). One side of the $ZnSnO_3$ belt was significantly thicker than the other side (thus, the term triangular-belts), as shown in Figure 1b. Further plane-view and cross-section SEM images of an individual triangular-belt are shown in Figure S1 in the Supporting Information. Figures 1c and 1d show high-resolution transmission electron microscopy (HRTEM) images and a corresponding selected-area diffraction (SAD) pattern, respectively. These images reveal that the nanobelt's growth direction was along the [001] axis. The SAD pattern was indexed to a rhombohedral structure of R3C space group with lattice constants of $a = 0.52622$ nm and $c = 1.40026$ nm.[19] Figure 1e illustrates the crystallographic structure; it consists of two octahedral cells of ZnO_6 and SnO_6 (see the left side of Figure 1e). The right side of Figure 1e shows that the ZnO_6 octahedral cell has three short oxygen bonds at 0.204 nm

Prof. J. M. Wu, C. Xu, Prof. Y. Zhang, Dr. Y. Yang,
Y. Zhou, Prof. Z. L. Wang
School of Materials Science and Engineering
Georgia Institute of Technology
Atlanta, GA 30332, USA
E-mail: zhong.wang@mse.gatech.edu
Prof. J. M. Wu
Department of Materials Science and Engineering
Feng Chia University
100 Wenhwa Rd, Seatwen, Taichung, 40724, Taiwan
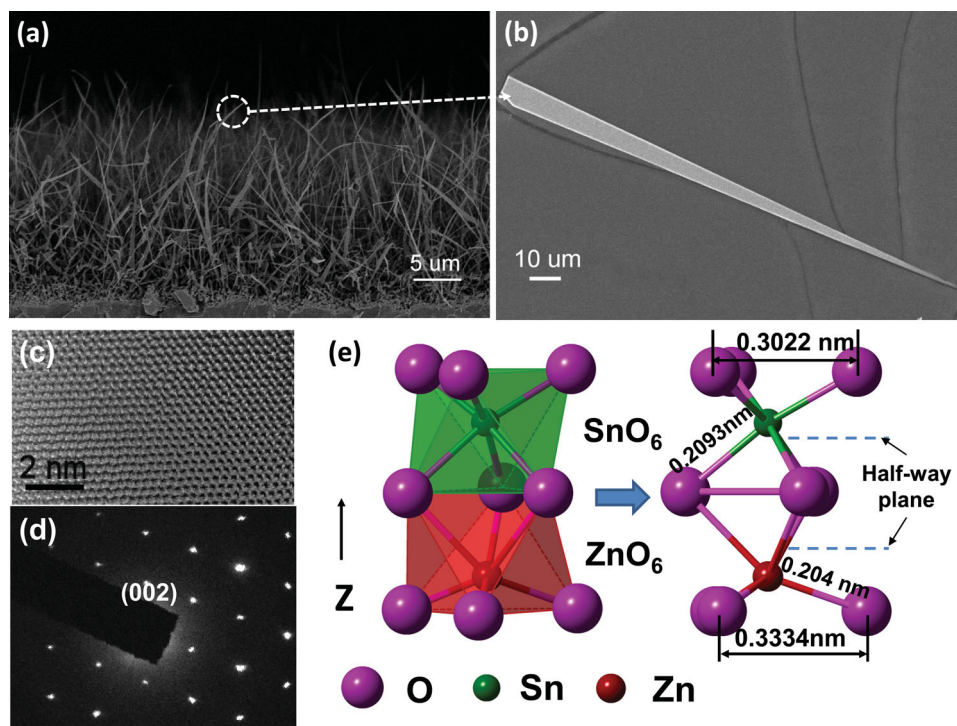
Figure 1. (a) Cross-sectional view of SEM image in ZnSnO$_3$ nanobelts (b) A triangular-belt with one side thicker than the other side and laying on a flat substrate. (c) High-resolution transmission electron microscopy image of an individual ZnSnO$_3$ nanobelt (d) Selected-area pattern image (SAD) shows the nanobelt's growth direction was [001]. (e) Crystallographic structure of ZnSnO$_3$ consisted of two octahedral cells of ZnO$_6$ and SnO$_6$ (left side). The right side crystallographic structure of ZnSnO$_3$ shows the bonding length of Zn-O and Sn-O along the z-axis.

and three long bonds at 0.2308 nm. The SnO$_6$ octahedra cell has three short bonds at 0.2008 nm and three long bonds at 0.2093 nm.[23] When the Zn and Sn atoms have an off-center displacement in ZnO$_6$ and SnO$_6$ octahedral cells, respectively, the total energy of the ZnSnO$_3$ decreases accordingly, and reaches its lowest energy when the displacement of Zn and Sn is around 0.05 nm and 0.02 nm, respectively. This lowest energy is the result of the competition between the short-range repulsions and long-range Coulomb forces.[24] There is unequal bonding length between the O-Sn-O (upper-site SnO$_6$ octahedral cell) and O-Zn-O (lower-site ZnO$_6$ octahedral cell) in the ZnSnO$_3$ structures; therefore, the Sn and Zn deviate from the octahedron center by nonequivalent amounts along the z-axis (see the right side of Figure 1e). The Zn atom is located in a large distorted position along the z-axis. This yields a noncentrosymmetric extended structure. When the ZnSnO$_3$ is applied under mechanical stress along the z-axis, a local dipole is created on the z-axis such that the extended structure exhibits a polar moment. This is the source of piezoelectricity in ZnSnO$_3$, which inspired us to comprehensively investigate the working principles and the output-power performance of a nanogenerator made from triangular-belt ZnSnO$_3$.

To understand the working principle of a composite triangular-belt nanogenerator, atomic force microscopy (AFM) was employed to investigate the geometric figure of the triangular-belt ZnSnO$_3$, which can be collected and well-dispersed on the surface of the substrate (see Figure S2, Supporting Information). **Figure 2**a shows a three dimensional (3D) image of an individual belt's tip, which obviously demonstrates that the

shape of the belt's taper is tightly attached on the substrate's surface. The tremendous difference between the two ends of the triangular belts makes their tips face downward into the substrate's surface. The cross sectional profiles of Figure 2b were taken using AFM. The measured position of the corresponding triangular-belt is shown in the inset of Figure 2b. The thickness of position A exceeds 8.5 μm, while that of position B is less than 1 μm. The width of position A and B is 19 and 4 μm, respectively. Thus, the belt's width and thickness in position A is 5 and 8 times larger, respectively, than that of position B. Figure 2c further demonstrates that the belt's tip was tightly adhered to the surface of the substrate as the thicker side of the belt was moved, resulting in a slight bend in the tip. This fact demonstrates that for all triangular-belts that have one side that is thicker than the other, the small size of belt's tip offers a high surface energy effect, which provides plenty of opportunity to make the triangular-belts tightly adhere to the substrate's surface. This significant phenomenon implies that the spontaneous polarization direction [001] in ZnSnO$_3$ was downward into the substrate, as the triangular-belts were highly dispersed on the substrate's surface.

Achieving flexibility and transparency using a simple and straightforward method, the nanogenerator was made from a unipolar composite of triangular-belt ZnSnO$_3$ permeated with PDMS (see Figure 2d) by a spin coating process (see Figure S1, Supporting Information and in the Experimental Section). Triangular-belts with a typical taper of ≈3° (see Figure 2e) were uniformly mixed with PDMS and spin-coated onto the surface of the substrate. After the triangular-belt PDMS solution
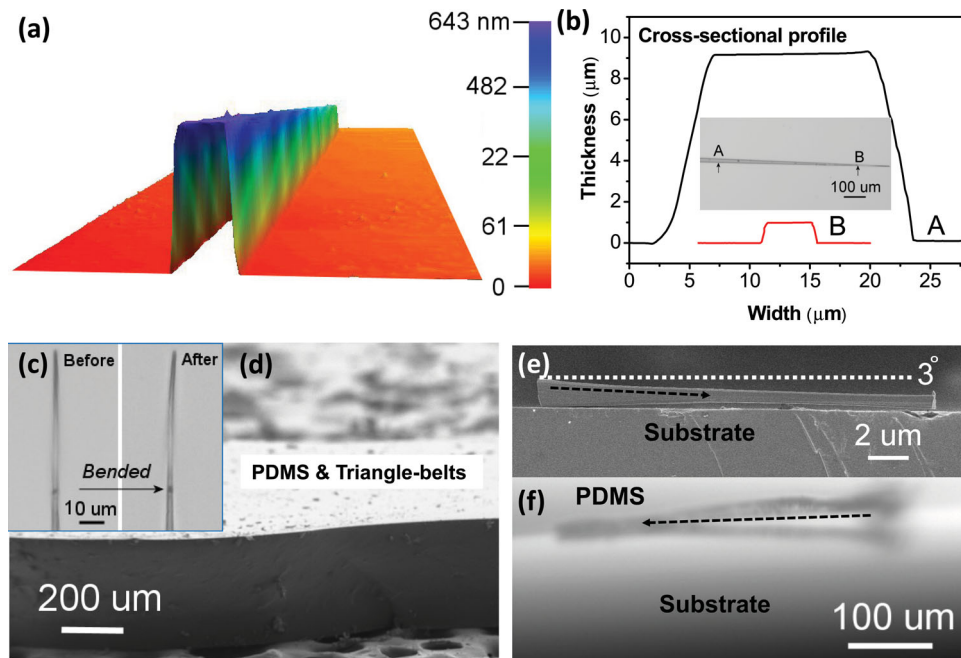
Figure 2. (a) 3D morphology of an individual triangular-belt. (b) A cross-sectional profile of a triangular-belt; inset image shows the corresponding positions of A and B. (c) Due to a surface energy effect, the tip is tightly adhered on the substrate's suface. After moved the thicker-side triangular-belt, its tip was slightly bended. (d) A composite triangular-belt PDMS. (e) A cross-sectional SEM image, which shows a triangular-belt lying on a flat substrate. The bottom side of the belt adheres to the substrate at ≈3°. The black-dashed arrowhead indicates that the triangular-belt tapers downward into the substrate. (f) A cross-sectional SEM image of a composite triangular-belt PDMS showing the triangular-belt's tip points into the substrate.

underwent two hours of solidification at a temperature of 110 °C, the belts' tips still pointed into the substrate and adhered to its surface, as seen in Figure 2f. Further cross-sectional images of the triangular-belt composite are shown in Figure S3a of the Supporting Information. This implies that all the triangular-belts sunk into the surface of the substrate when the triangular-belt PDMS underwent a solidification process. Although the multiple belts interlaced with each other, their tips still went downward into the substrate due to their unique geometric

figure. A plane-view image in Figure S3b exhibits that the triangular-belts were highly dispersed in the PDMS and lay evenly and horizontally on the surface of the substrate.

Based on our observations mentioned above, we propose that our triangular-belts may undergo a natural gravity-driven settling process (or sinking process). The belts are larger than 200 μm in length and 20 μm in width; therefore, they naturally sink into the surface of the substrate, as they were permeated with PDMS during a solidification process (shown in **Figures 3**a
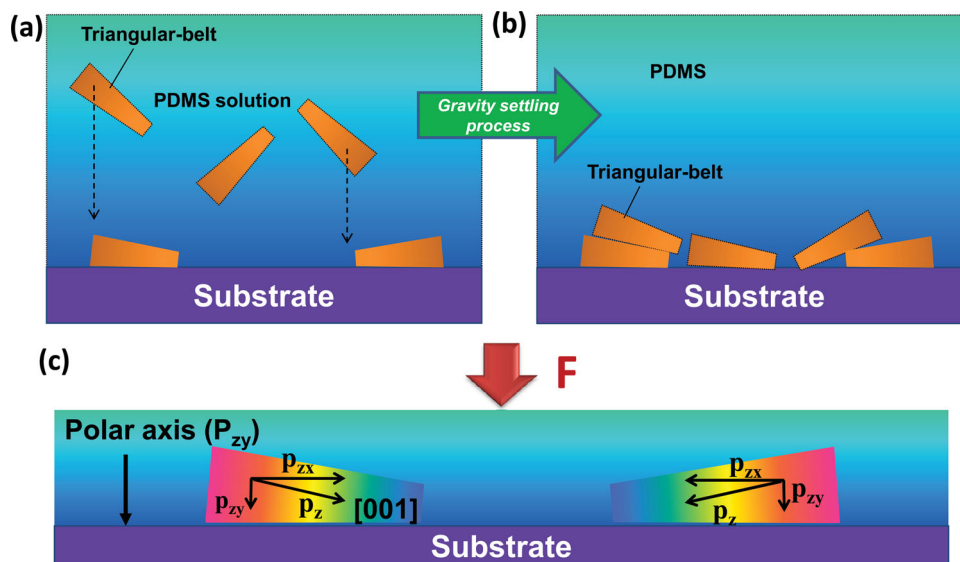
Figure 3. (a)–(b) Schematic diagram shows the sinking process as the triangular-belt PDMS solution undergoes a solidification process. (c) Schematic diagram of working principle for a triangular-belt nanogenerator (see details in text).

COMMUNICATION
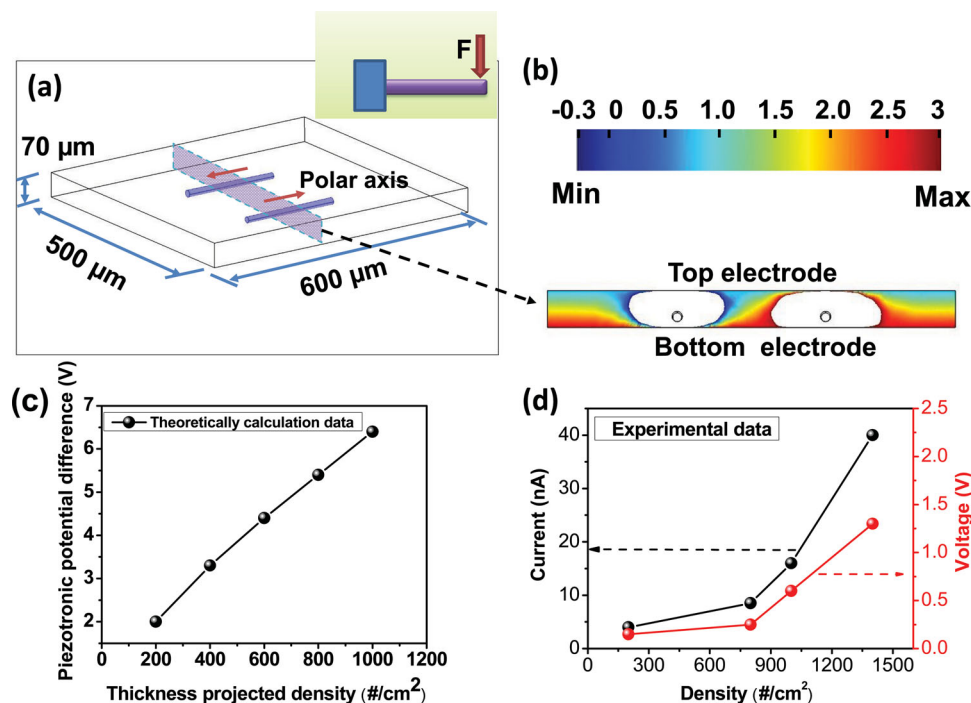
Figure 4. (a) A model for the potential distribution across the top and bottom electrodes of the nanogenerator with a pair of triangular-belts arranged as polar opposites. (b) The piezopotential distribution results from the theoretical model of a); (c) The piezotronic potential difference between the top and bottom electrodes of the nanogenerator as a function of triangular-belt density. (d) The experimental measured output current and voltage of a tandem-structure nanogenerator as a function of triangular-belt density.

and 3b). Basing it on the sinking process, we suggest a working principle for the triangular-belt composite nanogenerator, shown in the schematic diagram in Figure 3c. Because the triangular-belts were evenly deposited with random lateral orientation onto the flat surface of the substrate and were pointing downward into the substrate, Figure 3c suggests that the tips of two belts point towards each other. Therefore, the polar value along the z-axis (P_z) can be divided into two quantities: P_{zx} and P_{zy}, where P_{zx} is the component of P_z along the x-direction, and P_{zy} is the component of P_z along the y-direction. As such, we can assume that all polar quantities along the x-direction (e.g. P_{zx}) cancelled each other out because they pointed in opposite directions. In contrast, the projected quantities of all the belts along the y-direction (e.g. P_{zy}) were constructively accumulated because the tapers of the triangular-belts pointed into the substrate (see Figure 2e). Therefore, the unipolar accumulation along P_{zy} produced a substantial piezopotential in the direction perpendicular to the substrate's surface. This piezopotential exists throughout the thickness of the composite structure.

To demonstrate the working principle of the nanogenerator, theoretical calculations were carried out using the COMSOL software package.[25,26] For simplicity, the piezopotential was calculated without considering carrier concentration and finite conductance.[27,28] The crystal structure was R3C ZnSnO₃ with a triangular-belt morphology.[19] The piezoelectric stress and material constants are listed in Table S1 in the Supporting Information. The entire nanogenerator structure can be regarded as a capacitor-like plate composed of triangular-belts and a PDMS layer. The nanogenerator was taken as a cantilevered beam with

a periodical transverse force (F) applied at the top edge of its one fixed end (see inset, **Figure 4**a). On the basis of our theoretical calculation under the first-order approximation, the calculation of the coupling effect between the induced charges and the piezoelectric field in the electric plates was omitted. The piezopotentials inside the two belts have opposite signs in the P_{zx} axis (see Figures 4a and 3c). The theoretical model of a nanogenerator (Figure 4a) was applied under a compressive strain of 0.1%, and the calculated result of the piezopotential distribution is shown in the bottom portion of Figure 4b. Figure 4b shows a separation in the charge centers in the direction perpendicular to the surface of the substrate. This is the working principle that induces charges across the top and bottom electrodes of the nanogenerator. When a compressive strain of ≈0.1% was applied, an induced potential difference of ≈3 V was generated between the top and bottom electrodes, as shown in the top part of Figure 4b. As shown in Figure 4c, the calculated data further predicts that the output electric potential difference between the top and bottom electrodes was proportional to the density of triangular-belts which had been dispersed on the surface of the substrate.

Demonstrating that the experimental results confirmed the theoretical calculations, the experiments were performed with a variety of film stacks having 1, 4, 5, and 7 layers to investigate the output power of the tandem-structure nanogenerator using a cyclic deposition process (see detail in Figure S1, Supporting Information). On average, each layer contained approximately 200 triangular-belts per square centimeter. The more layers the nanogenerator had, the more voltage and current it put out, as

© 2012 WILEY-VCH Verlag GmbH & Co. KGaA, Weinheim
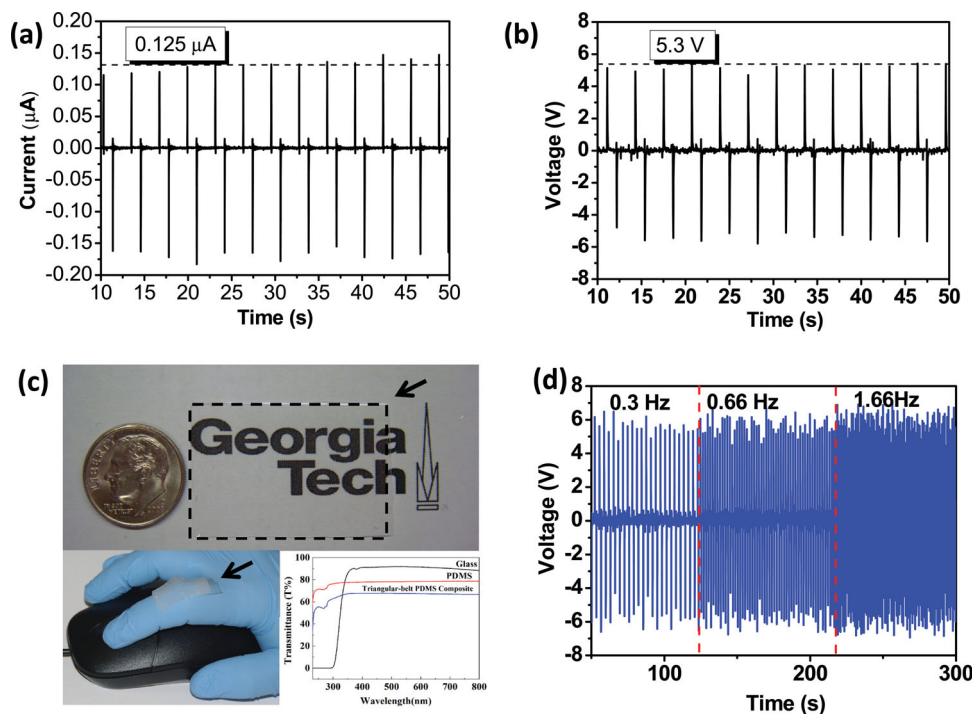
Figure 5. (a) Electrical output current of triangular-belt composite nanogenerator, and (b) output voltage. (c) The photograph of a composite triangular-belts PDMS attached on a paper that indicates the high transparency of the nanogenerator; inset lower left-hand-side image showing a highly flexible nanogenerator; inset lower right-hand-side image showing the transmittance spectrum as a function of wavelength. (d) The nanogenerator shows good stability with an increase in driving frequency.

shown in Figure 4d. A nanogenerator with 7 layers achieved around 1.3 V of voltage and 40 nA of current. The actual power was generally lower than the theoretical predicted power. This was due to the screening effect of the free charge carriers and the finite conductance,[29,30] both of which may affect the power that is actually put out. In addition, as found in our previous work,[15] the actual output power can be related to the size effect. However, the theoretical calculations were in semi-quantitative agreement with our experimental observations. This phenomenon was generally consistent with our previous work.[31]

To simplify the fabrication process and to avoid a complicated cyclic deposition process, 1:100 in weight percentage (wt%) of triangle-belts and PDMS were mixed together to fabricate a flexible and transparent nanogenerator. Based on the working principle of the triangular-belt composite nanogenerator, the actual output current and voltage are shown in **Figures 5**a and 5b, respectively. The output current achieved 0.13 µA, and the output voltage exceeded 5.3 V. Figure 5c shows that the nanogenerator was highly transparent, stretchable, and flexible (see Figure 5c, lower left-hand side), which exhibits great advantages in the applications of commercial portable devices. The high transparency of the nanogenerator achieved ≈68% (see Figure 5c, lower right-hand side). Figure 5d shows that the output voltage of the nanogenerator was not significantly changed when the driving frequency was increased from 0.3 to 1.6 Hz. Because the results exhibited high stability, the triangular-belt $ZnSnO_3$ nanogenerator can harvest energy from irregular excitations such as those in our living environment. Based on our theoretical model and experimental results, our

lead-free $ZnSnO_3$ nanogenerator has proven its tremendous potential for energy harvesting. It is likely that this demonstration can be scaled up for industrial applications by simple and cost-effective processes.

In summary, a nanogenerator has been developed using lead-free R3C $ZnSnO_3$ triangular-belts. By introducing a mechanical deformation of ≈0.1%, the nanogenerator generated a current and voltage of 0.13 µA and 5.3 V, respectively. Its output power density reached a maximum of ≈11 µW·cm^{-3}. The working principle relies on the geometry of the unipolar assembly (P_{zy}) in the triangular-belt structure, which produces a piezotronic potential across the nanogenerator, thereby driving a flow of induced charges between the top and bottom electrodes. Both theoretical predictions and experimental results showed that the output electric potential difference between the top and bottom electrodes was proportional to the density of the triangular-belts. This is a novel discovery as it is the first demonstration of high output power from a lead-free $ZnSnO_3$ nanogenerator that employed a simple, cost-effective, and scalable technology which can be developed for further industrial applications.

Experimental Section

Material Preparation: Zn and Sn (0.5 g, purity: 99.9%) with graphite powder were used as source materials; they were placed in the center zone of a quartz reactor to perform a carbon-thermal reaction. The reaction took place at a constant temperature of 900 °C at 10–20 Torr for three hours. The argon and oxygen gas flow rates were 200 sccm and 10–20 sccm, respectively.

COMMUNICATION

Device Fabrication: First, the poly(imide) (PI) substrate was deposited by Cu/Cr to serve as a bottom electrode. To prepare the nanogenerator, the triangular-belt $ZnSnO_3$ and PDMS solution were mixed together at a proportion of 1:100 (by weight percentage) and deposited onto a PI substrate using a spin coating process (200–500 rpm, 60 s). Subsequently, an additional layer of polydimethylsiloxane (PDMS) was coated over the nanogenerator to keep the nanogenerator robust under mechanical stress or deformation. A Cu/Cr layer was deposited on the PDMS film to serve as a top electrode. The effective working area of the nanogenerator was about 1.5 cm × 2 cm. The thickness of the triangular-belt PDMS composite was around 200 μm. A variety of films stacks of 1, 4, 5, and 7 layers were prepared as control samples. The triangular-belt PDMS solution was deposited onto a PI substrate using the cyclic deposition off a spin coating process (2000 rpm, 60 s), forming a tandem-structure nanogenerator (for details of the process, see Figure S1 and Figure S4, Supporting Information).

Material Characterization: A thin-film X-ray diffractometer (Bruker, D8 SSS), high-resolution transmission electron microscope (HRTEM, JEOL JEM-3000F, operated at 300 kV), and field emission scanning electron microscope (FESEM, HITACHI S4800, operated at 3 kV) were used for materials characterization.

Electrical Measurements: The output signal of the nanogenerator was measured with the use of a low-noise voltage preamplifier (Stanford Research System Model SR560) and a low-noise current preamplifier (Stanford Research System Model SR570).

Supporting Information

Supporting Information is available from the Wiley Online Library or from the author.

Acknowledgements

[1] T. Kimura, T. Goto, H. Shintani, K. Ishizaka, T. Arima, Y. Tokura, *Nature* **2003**, *426*, 55.

[2] N. Hur, S. Park, P. A. Sharma, J. S. Ahn, S. Guha, S. W. Cheong, *Nature* **2004**, *429*, 392.

[3] M. D. Maeder, D. Damjanovic, N. Setter, *J. Electroceram.* **2004**, *13*, 385.

[4] D. W. Wu, Q. F. Zhou, X. C. Geng, C. G. Liu, F. Djuth, K. K. Shung, *IEEE Trans. Ultrason. Ferr.* **2009**, *56*, 2304.

[5] D. N. Shen, J. H. Park, J. H. Noh, S. Y. Choe, S. H. Kim, H. C. Wikle, D. J. Kim, *Sens. Actuators, A* **2009**, *154*, 103.

[6] Y. F. Li, R. Horowitz, R. Evans, *IEEE Trans. Magn.* **2003**, *39*, 932.

[7] Z. L. Wang, J. H. Song, *Science* **2006**, *312*, 242.

[8] J. M. Wu, Y. R. Chen, *J. Phys. Chem. C* **2011**, *115*, 2235.

[9] Q. Yang, W. H. Wang, S. Xu, Z. L. Wang, *Nano Lett.* **2011**, *11*, 4012.

[10] X. D. Wang, J. Zhou, J. H. Song, J. Liu, N. S. Xu, Z. L. Wang, *Nano Lett.* **2006**, *6*, 2768.

[11] Y. Yang, W. X. Guo, Y. Zhang, Y. Ding, X. Wang, Z. L. Wang, *Nano Lett.* **2011**, *11*, 4812.

[12] J. Zhou, Y. D. Gu, P. Fei, W. J. Mai, Y. F. Gao, R. S. Yang, G. Bao, Z. L. Wang, *Nano Lett.* **2008**, *8*, 3035.

[13] R. S. Yang, Y. Qin, L. M. Dai, Z. L. Wang, *Nat. Nanotechnol.* **2009**, *4*, 34.

[14] S. Xu, B. J. Hansen, Z. L. Wang, *Nat. Commun.* **2010**, *1*, 93.

[15] G. Zhu, R. S. Yang, S. H. Wang, Z. L. Wang, *Nano Lett.* **2010**, *10*, 3151.

[16] J. H. Jung, M. Lee, J. I. Hong, Y. Ding, C. Y. Chen, L. J. Chou, Z. L. Wang, *ACS Nano* **2011**, *5*, 10041.

[17] M. Nakayama, M. Nogami, M. Yoshida, T. Katsumata, Y. Inaguma, *Adv. Mater.* **2010**, *22*, 2579.

[18] J. Zhang, K. L. Yao, Z. L. Liu, G. Y. Gao, Z. Y. Sun, S. W. Fan, *Phys. Chem. Chem. Phys.* **2010**, *12*, 9197.

[19] Y. Inaguma, M. Yoshida, T. Katsumata, *J. Am. Chem. Soc.* **2008**, *130*, 6704.

[20] J. A. Christman, R. R. Woolcott, A. I. Kingon, R. J. Nemanich, *Appl. Phys. Lett.* **1998**, *73*, 3851.

[21] J. M. Wu, X. Chen, Y. Zhang, Z. L. Wang, *ACS Nano* **2012**, *6*, 4335.

[22] J. M. Wu, C. Y. Chen, Y. Zhang, K. H. Chen, Y. Yang, Y. Hu, J. H. He, Z. L. Wang, *ACS Nano* **2012**, *6*, 4369.

[23] C. A. Hoel, J. M. G. Amores, E. Moran, M. A. Alario-Franco, J. F. Gaillard, K. R. Poeppelmeier, *J. Am. Chem. Soc.* **2010**, *132*, 16479.

[24] J. Zhang, K. L. Yao, Z. L. Liu, G. Y. Gao, Z. Y. Sun, S. W. Fan, *Phys. Chem. Chem. Phys.* **2010**, *12*, 9197.

[25] Y. Zhang, Y. Liu, Z. L. Wang, *Adv. Mater.* **2011**, *23*, 3004.

[26] http://www.comsol.com/showroom/gallery/114/, Comsol Model Gallery (Semiconductor Diode), accessed April 2011.

[27] Y. Gao, Z. L. Wang, *Nano Lett.* **2009**, *9*, 1103.

[28] G. Mantini, Y. F. Gao, A. D'Amico, C. Falconi, Z. L. Wang, *Nano Res.* **2009**, *2*, 624.

[29] Z. Z. Shao, L. Y. Wen, D. M. Wu, X. A. Zhang, S. L. Chang, S. Q. Qin, *J. Appl. Phys.* **2010**, *108*, 124312.

[30] Y. Zhang, Y. Liu, Z. L. Wang, *Adv. Mater.* **2011**, *23*, 3004.

[31] Y. F. Hu, Y. Zhang, C. Xu, G. A. Zhu, Z. L. Wang, *Nano Lett.* **2010**, *10*, 5025.